CONDENSATION HEAT TRANSFER CHARACTERISTICS OF THE ALKALI METAL THERMAL TO ELECTRIC CONVERTER (AMTEC) POROUS WICK CONDENSER

by

Lan XIAO[a*], Deng ZHANG[a], Shuang-ying WU[b], and Hui-jia YU[c]

[*a] Key Laboratory of Low-Grade Energy Utilization Technologies and Systems, Ministry of Education, Chongqing University, Chongqing, China
[b] College of Power Engineering, Chongqing University, Chongqing, China
[c] Chongqing Energy College, Chongqing, China

Original scientific paper
https://doi.org/10.2298/TSCI170727069X

An axisymmetric 2-D mathematical model was established and the volume of fluid +method was adopted to numerically investigate the condensation heat transfer process of alkali metal in the alkali metal thermal to electric converter (AMTEC) porous wick condenser. The steady-state physical fields of working medium were obtained and the impacts of some relevant parameters including geometrical and operational parameters on condensation heat transfer characteristics were discussed. The results show that the thickness of the liquid sodium increases along the radial direction. The temperature distribution in liquid phase is approximately linear. The condensation rate at the phase-change interface decreases along the radial direction, and the cold end heat flux, q, increases initially and then decreases along the radial direction. The porous wick condenser has very limited self-adaptive ability once the mass flow rate, M_{in} , exceeds some critical value. In addition, there is a corresponding $T_{w,}$ for a certain M_{in} to ensure the stable phase-change interface. The performance of AMTEC can be enhanced by reducing the distance between artery and cell wall.

Key words: *AMTEC, porous wick condenser, condensation heat transfer, numerical simulation*

Introduction

The alkali metal thermal to electric converter (AMTEC), as its name suggests, is a thermally regenerative, electrochemical device for the direct conversion of heat to electrical power using alkali metal as working medium. In recent years, AMTEC has attracted much concern due to its unique advantages such as relatively high conversion efficiency (20-30%), simple configuration, no noise and good adaptability to a variety of heat sources including nuclear energy, solar energy, heat of combustion, *etc*. [1, 2]. A perspective view in partial cross-section of AMTEC cell using sodium as working media is given in fig. 1 [3]. The AMTEC cell is based on an ionic selective membrane, *i. e*., *β''*-alumina solid electrolyte (BASE), which only allows the sodium ions to pass through. The working principle can be described briefly as: the liquid sodium in capillary evaporator is heated by the heat input from an external source at the hot end and becomes high pressure sodium vapor. Then, the vapor is delivered to the BASE/anode interface where ionization of sodium metal occurs because of the thermodynamic potential across the BASE ($Na \rightarrow e + Na^+$). Only the sodium ions can diffuse through the BASE to the

*Corresponding author, e-mail: xiaolannancy@cqu.edu.cn

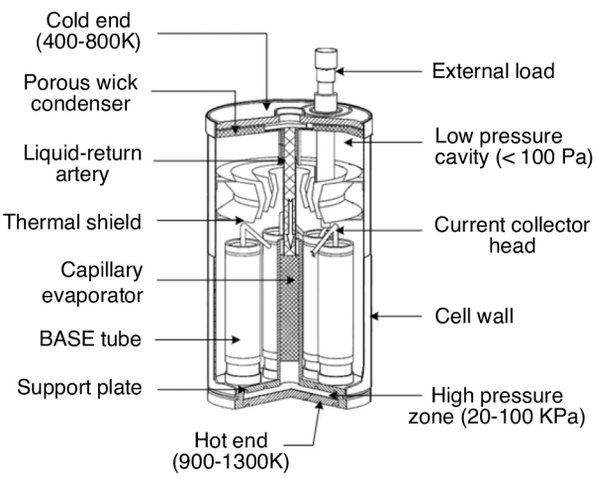

Figure 1. A perspective view in partial cross-section of AMTEC cell [3]

cathode, the electrons circulate through the external load producing electrical work and then reach the cathode surface where they recombine with the sodium ions to reform sodium atoms at the BASE/cathode interface ($Na^+ + e \rightarrow Na$). The sodium, in vapor form, passes through the low pressure cavity and reaches the condenser surface, where it gives up the latent heat of condensation to become liquid, and then recycle to the liquid-return artery by capillary action of the evaporator [2].

The authors once did a thorough review of the state of the art in the research and development of the AMTEC [2]. It was revealed that, the researches about AMTEC mainly focus on its overall performance test and optimization [4, 5], application fields [6], material and structure design [7, 8], numerical simulation of flow and thermal performance, heat loss, as well as the heat and mass transfer characteristics of capillary evaporator [9, 10]. Comparatively speaking, little attention has paid to the porous wick condenser. In fact, the porous wick condenser, which controls the circulation flow of working medium and the heat transfer inside the AMTEC, is equally important as the evaporator. On the other hand, since the heat-rejection temperature of AMTEC namely the operation temperature of condenser is 400-800 K, it is cost-efficient to utilize the heat from the AMTEC condenser. If the rejected heat from the condenser is recycled, it not only can improve the overall conversion efficiency, but also can avoid thermal pollution to the environment. However, little effort has been poured into how to utilize the rejected heat of AMTEC condenser, and only a conceptual design of cascading AMTEC/TEC system has been proposed [6, 11]. As an exploratory study, the authors have proposed a parabolic dish/AMTEC solar thermal power system and evaluated its overall thermal-electric conversion performance. It should be noted that, the evaluation results were obtained on the basis of the existing empirical or semiempirical correlations. In other words, the internal heat transfer characteristics of AMTEC components including the condenser were not fully considered. Nevertheless, for a cascading system comprised of AMTEC and other heat utilization device, the heat rejection from AMTEC condenser is actually the heat source of other heat utilization device. Thus, it is necessary to research into the sodium vapor condensation heat transfer in AMTEC porous wick condenser, so as to provide guidance for the optimization of coupling conditions.

According to our analysis, for the AMTEC condenser, the sodium vapor condensates in the porous wick condenser which essentially belongs to condensation problem in porous media. Currently, the work on the condensation problem in porous medium, according to the surface geometry can be classified as vertical plate [12], horizontal plate [13], disc [14], circular tube [15], elliptical tube [16], *etc*. Whereas, the AMTEC wick condenser is circular ring structure, which differs from the existing research. In view of this, this article takes the AMTEC wick condenser as research subject, and establishes a physical and mathematical model to investigate the condensation heat transfer characteristics of sodium in AMTEC porous wick condenser numerically. One should notice that, the present paper emphasizes the detail research of an

AMTEC component namely the porous wick condenser, which has never been reported in the existing work. The motivation behind our work is to provide theoretical guidance for the design, operation, optimization and evaluation of AMTEC itself or AMTEC cascading with other heat utilization device.

The physical and mathematical model

Physical model

The sketch diagram of AMTEC porous wick condenser is shown in fig. 2, a layer of porous wick such as mesh pad is arranged at the cold end internal surface. Considering the symmetry of the condenser, an axisymmetric 2-D model, which consists of porous wick and a part of low pressure cavity, is established in the cylindrical co-ordinate as shown in fig. 3. Both the low pressure cavity (F-G) and the porous wick (C-F) are 10 mm in axial length, while the distance between artery and cold end, L_{cd}, is 5 mm. The radiuses of liquid-return artery and AMTEC cell are 2 mm (D-E) and 17 mm (B-C), respectively. The porous wick is made of Titanium whose properties are porosity $\varepsilon = 0.4$, effective aperture $r_p = 2\times10^{-5}$ mm, permeability $K = 4.55\times10^{-12}\text{m}^2$.

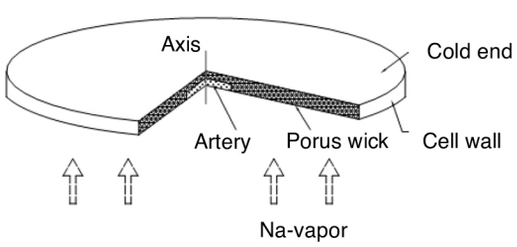

Figure 2. Sketch diagram of AMTEC porous wick condenser

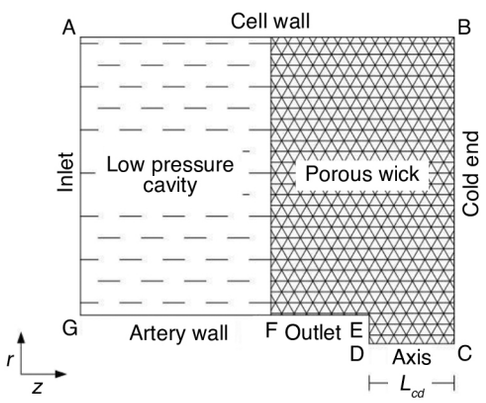

Figure 3. Physical model of AMTEC porous wick condenser

Mathematical model

The VOF model has been widely used to solve the problems involving free interface capturing and phase change heat transfer in microscale channels [17, 18]. As a consequence, in our study, the VOF model is adopted to investigate the condensation heat transfer of sodium vapor in AMTEC porous wick condenser. Some hypotheses are employed in mathe-matical modeling.

- The porous media is homogeneous and isotropic, and meets the local thermal equilibrium assumption, namely the temperature of solid skeleton and fluid is equal.
- There is no temperature difference between liquid and vapor in phase change interface, namely, the liquid membrane temperature is equal to the saturated steam temperature.
- The physical properties of liquid film and porous media are constant within the range of operating temperature.
- The flow is laminar in all regions, ignoring the effects of gravity and capillary force.

Continuity equation:

$$\frac{\partial}{\partial t}(\varepsilon\rho_{\mathrm{f}}) + \nabla\cdot(\rho_{\mathrm{f}}\vec{V}) = 0 \tag{1}$$

Momentum equation:

$$\frac{\rho_f}{\varepsilon}\frac{\partial \vec{V}}{\partial t}+\frac{\rho_f}{\varepsilon^2}(\vec{V}\cdot\nabla)\,\vec{V}=-\nabla P-D\frac{\mu}{K}\vec{V}+\frac{\mu}{\varepsilon}\nabla^2\vec{V} \tag{2}$$

where D is a variable differentiating the low pressure cavity ($D = 0$) and the porous wick ($D = 1$) zone.

Energy equation:

$$\overline{\rho c}\frac{\partial T}{\partial t}+\rho_f c_f(\vec{V}\cdot\nabla)\,T=\nabla\cdot(\lambda_{eff}\nabla T)+S_h \tag{3}$$

In VOF model, tracking of the interface between the phases is accomplished by the solution of the continuity equation for the volume fraction of the secondary phase. In present paper, the liquid and vapor are set as the primary and secondary phases respectively [19], thus the VOF equation is written:

$$\frac{\partial \alpha_v}{\partial t}+\nabla\cdot\left(\alpha_v\vec{V}\right)=-\frac{\dot{m}}{\rho_v} \tag{4}$$

where $\dot{m}$ is the mass production rate due to condensation and α_v is the volume fraction factor of the vapor. If $\alpha_v = 1$, the region is occupied by pure vapor, while if $\alpha_v = 0$ the region is pure liquid. The value of α_v varies between 0 and 1, and the volume fraction of liquid is defined as $\alpha_l = 1 - \alpha_v$.

The properties in the equations above are given as the volume-fraction-averaged form, which can be written:

$$\rho_f=\alpha_v\rho_v+(1-\alpha_v)\rho_l \tag{5}$$

$$\mu=\alpha_v\mu_v+(1-\alpha_v)\mu_l \tag{6}$$

$$\lambda_{eff}=[\alpha_v\lambda_v+(1-\alpha_v)\lambda_l]\varepsilon+(1-\varepsilon)\lambda_s \tag{7}$$

$$\overline{\rho c}=[\alpha_v\rho_v c_v+(1-\alpha_v)\rho_l c_l]\varepsilon+(1-\varepsilon)\rho_s c_s \tag{8}$$

$$c_f=[\alpha_v c_v+(1-\alpha_v)c_l]/\rho_f \tag{9}$$

Phase change model:

The key to simulate the condensation process is the determination of the condensation rate and the latent heat transfer, which is usually achived by adding the source terms in the governing equation. In view of the numerical implementation and convergence, Lee model, based on the kinetic gas theory, is adopted to describe the source terms in this paper [19]. Mass and energy source terms can be written as follows:

$$\dot{m}=-\beta\alpha_l\rho_l\frac{T-T_{sat}}{T_{sat}}\quad(T\geq T_{sat}) \tag{10}$$

$$\dot{m}=-\beta\alpha_v\rho_v\frac{T_{sat}-T}{T_{sat}}\quad(T<T_{sat}) \tag{11}$$

$$S_h=\dot{m}h_{fg} \tag{12}$$

where T is the local temperature of discrete control volume, β – the mass transfer intensity factor (s^{-1}), an excessively large β causes numerical convergence problem, while a too small value leads to a significant deviation between the interfacial temperature and the saturation temperature. Researchers have used a very wide range of β value, for instance, Yang *et al*. [20] performed VOF simulation of boiling in a coiled tube using the value $\beta = 100\ s^{-1}$. Liu *et al*. [19] analyzed the film condensation between vertical parallel plates using VOF model, in which β is set as $5000\ s^{-1}$. Da Riva and Del Col [21] even set β as $1.0\cdot10^7\ s^{-1}$ for a high mass velocity of $G = 800\ kg\cdot m^{-2}\cdot s^{-1}$. These values were found by a trial-and-error procedure to numerically maintain the interface temperature close to saturation temperature. The coefficient β is set as $6\cdot10^6\ s^{-1}$ in present work.

Boundary condition:

A-G (inlet):

$$T = T_{sat},\ M = M_{in},\ \alpha_v = 1 \tag{13}$$

D-E (outlet):

$$P = P_{out},\ \partial T/\partial z = 0,\ \partial \alpha_v/\partial z = 0 \tag{14}$$

B-C (cold end):

$$T = T_w,\ V = 0 \tag{15}$$

C-D (axis):

$$\partial P/\partial r = 0,\ \partial T/\partial r = 0 \tag{16}$$

A-B (cell wall), E-G (artery wall):

$$\partial T/\partial r = 0 \tag{17}$$

The governing equations were numerically solved by finite volume method, using the commercial CFD package ANSYS FLUENT 15.0. User Defined Functions codes were built based on Lee model to simulate the condensation process. Considering the dynamic behavior of the two-phase flow, transient calculations were carried out with a time step of $1\cdot10^{-6}$ s for all cases. The time step was selected based on the Courant number, which is the ratio of the time step to the time a fluid takes to move across a cell. For the time step of $1\cdot10^{-6}$ s, the Courant number is less than 0.1 which ensures the stability of the calculation. Pressure-implicit with splitting of operators algorithm is applied to the pressure and velocity coupling solution. Pressure staggering option scheme was used for pressure discretization while the second order upwind scheme is employed to the momentum and energy equation. Besides, geo-reconstruct scheme was recommended to the volume fraction discretization. When the mass flow rate of inlet and outlet is equal, and other physical fields do not change over time, the condenser is considered in steady state operation. The physical properties of sodium and porous wick can be found in [22].

Crid independent test and model validation

Structured grid has been adopted to the meshing process, and a local mesh refined method is used for the region where the condensation probably occurs, so as to capture the phase change interface more accurately. In order to test the grid dependency on the model, three groups of grid number are considered. As shown in tab. 1, the minimum film thickness, δ_{min}, and the average temperatures of outlet, T_{out} , are monitored, taking a typical working condition, *i. e.*, M_{in}= 3 mg/s, T_{sat} = 650 K, T_w = 646 K as example. To balance the accuracy and arithmetic speed, the total grid number of 108900 is chosen to solve the mathematical equations.

Table 1. Grid independency test

Grid number	98000	108900	122800
δ_{min} / [mm]	9.76	9.78	9.78
T_{out} / [K]	647.11	647.10	647.10

To verify the reliability of the current model in solving the condensation problem in porous media, a plat type condenser with porous wick using methyl alcohol as working fluid was calculated. Geometric dimensions and operating parameters of the condenser are the same as those in [23]. Comparing the distributions of vapor phase volume fraction and temperature shown in fig. 4, the results of the present model agree well with those in [23] and the geo-reconstruct scheme used in this paper effectively avoids fuzzy interface. Qu *et al*. [24] conducted a visual experimental research on the same plat type condenser with porous wick, and the shape of the liquid film at steady state is given in fig. 5. The black area represents the liquid phase, while the white area represents the vapor phase. In the visualization experiment, the velocity of the inlet is 0.6 m/s and the temperature of the inlet is 337.15 K. The temperature difference between the inlet and cold wall is set to be 10 K. It is

observed that interfaces of present model and Qu *et al*. [24] show similar shape. Hence, the calculation model provided in this paper can be used with confidence.

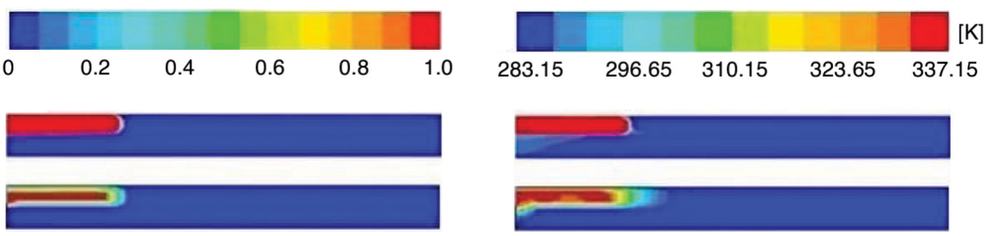

(a) Distribution of vapor volume fraction (b) Temperature distribution

Figure 4. Results comparison between present work (top) and [23] (bottom) *(for colour image see journal web site)*

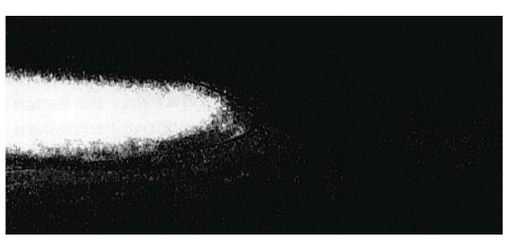

Figure 5. Visualization experimental result of [24]

Results and discussion

Physical fields in porous wick condenser

The steady-state distributions of liquid phase volume fraction, temperature, velocity and pressure of working medium were obtained under the condition of M_{in} = 3 mg/s, T_{sat} = 650 K, T_w = 646 K as shown in fig. 6. Initially, the porous wick zone is filled with liquid sodium, while the low pressure cavity is full of saturated sodium vapor.

The distribution of liquid phase volume fraction is given in fig. 6(a), where the blue and red regions represent the sodium vapor and liquid, respectively. It can be found that a stable vapor-liquid interface is maintained nearby the surface of the porous wick, that is to say, all sodium vapor starts to condensate once enter the porous wick region. It should be noted that the thickness of the sodium liquid film, δ, increases continuously along the radial direction, r, as shown fig. 7, however, the range of this variation is less than 0.2 mm, thus the porous wick condenser shown in fig. 6(a) seems like to be filled with liquid sodium with the naked eye. Moreover, the liquid-vapor two phase region is extremely thin which agree with Shi *et al*. [25] conclusion that thickness of the transition region from vapor to liquid is very thin, only about 1-2 molecular diameter.

Figure 6(b) shows the distribution of the temperature. Clearly, temperature in vapor phase is constant, while the temperature distribution in the liquid phase is linear approximately. The reasons can be explained as follows. In low pressure cavity, the temperatures of the inlet vapor and the phase change interface are both assumed to equal to the saturated steam temperature, T_{sat}, thus there is no temperature gradient. As for the porous wick region, the effective thermal conductivity, λ_{eff}, is large enough (λ_{eff} = 46.7 $W \cdot m^{-1} \cdot K^{-1}$), on the other hand, the velocity of liquid sodium after condensation is extremely small (in the order of 10^{-5} m/s), as shown in fig. 6(c). Hence, the latent heat releases mainly through heat conduction, the influence of convection is negligible, so that the temperature is linearly distributed along the axial direction.

The velocity contour combined with the pathline is shown in fig. 6(c). It can be found that the velocity of the sodium vapor increases significantly at the porous wick surface near the liquid-return artery, whereas, the velocity decreases at the porous wick surface near the cell wall. According to the pathline, the sodium vapor tend to flow towards the region around the liquid-return artery. The previous facts mean that the mass-flow rate of the sodium vapor flow is not evenly distributed but decreases along the radial direction. Consequently, a similar trend is

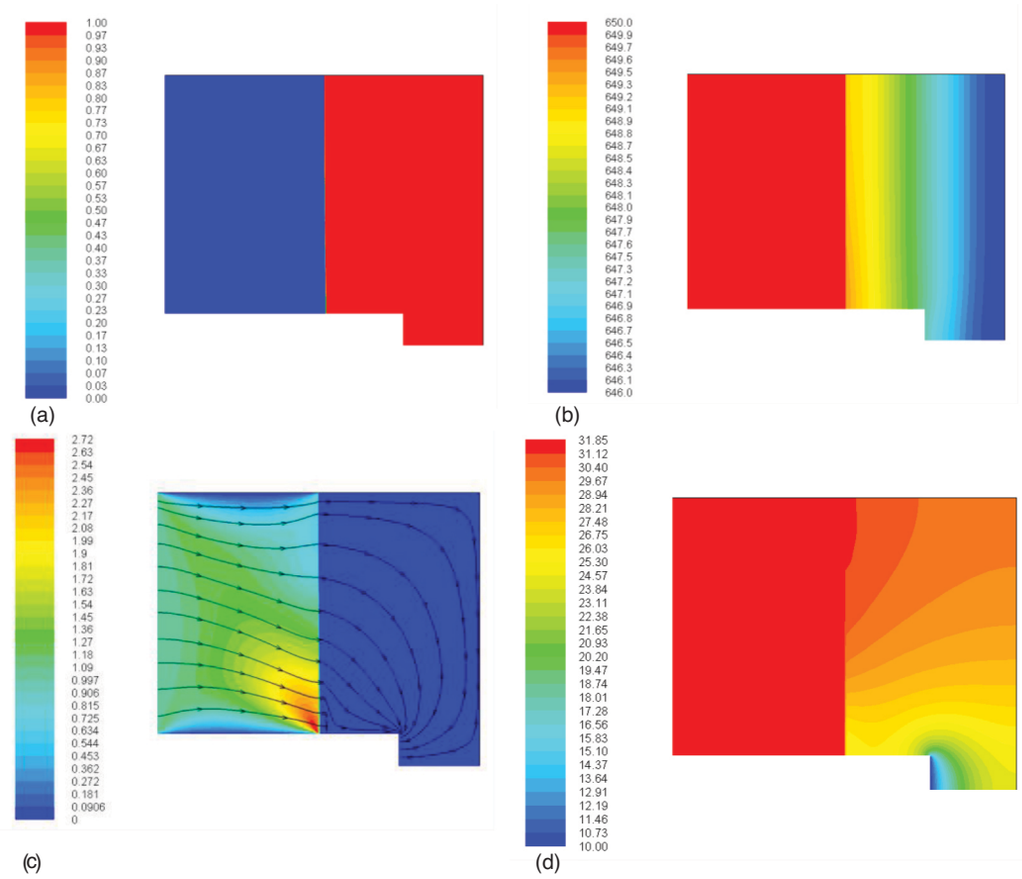

Figure 6. Contours of phase (a) liquid phase volume fraction, (b) temperature, (c) velocity, and (d) pressure *(for colour image see journal web site)*

presented in the distribution of cold end heat flux, q, as shown in fig.7. However, it should be noted that the cold end heat flux increases initially ($0 < r < 7$, mm) and then decreases ($7 < r < 17$, mm) along the radial direction rather than monotone decreasing. This trend is mainly due to the fact that the heat transfer area between the outlet and the cold end gets increased which reduces the local heat flux, moreover, all the cooling sodium liquid eventually converges to the outlet causing a lower temperature near the outlet. In addition, under a steady-state operation condition the heat released from the cold end should be equal to the condensation latent heat based on theoretical analysis.

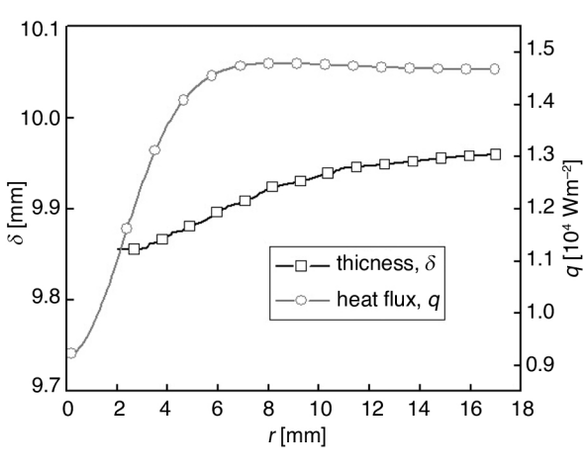

Figure 7. Distribution of δ and q along the radial direction

When the mass-flow rate of inlet M_{in} is 3 mg/s, the total heat transfer rate, Q, should be 13.2 W. Integrating the cold end heat flux along radial direction, the total heat transfer rate, Q', is calculated to be 12.9 W, namely $Q \approx Q'$ which further illustrates the rationality of the present model.

Figure 6(d) shows the contour of pressure, usually, the pressure in the low pressure cavity is less than 100 Pa. The effect of the heat shield of AMTEC is not considered, so that the flow resistance in low pressure cavity is very small and the pressure of vapor phase is almost unchanged. Because of the assumption that the flow is laminar, the influence of inertia resistance is ignored, the flow resistance in the porous wick is only derived from the viscous stress. In the region around the liquid-return artery, the flow resistance is much smaller, thus more sodium vapor tends to condensate at the surface nearby liquid-return artery.

The effect of mass-flow rate

In actual operation, the mass-flow rate of an AMTEC tends to fluctuate with the hot end heat input. The more heat is supplied to the hot end, the greater the amount of sodium vapor flowing out of the capillary evaporator. Consequently, the condenser should be self-adaptive to ensure that sodium vapor condensates completely in the porous wick, and only liquid sodium returns to the artery, otherwise the loop of the whole AMTEC may be interrupted.

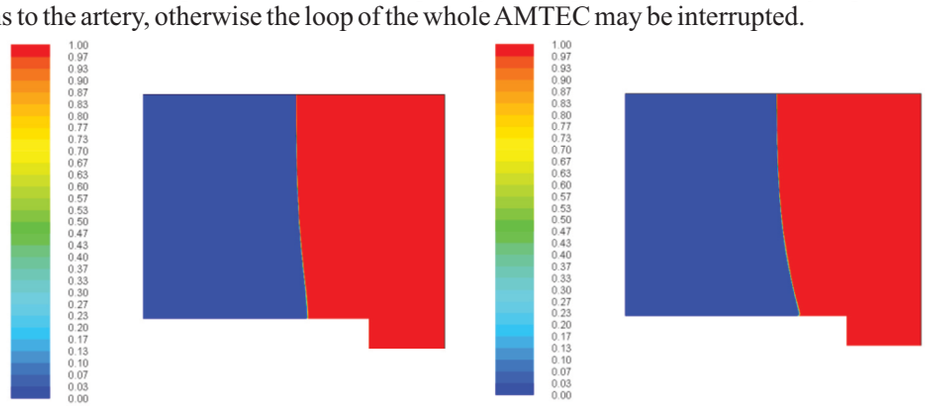

Figure 8. Contours of liquid phase under different M_{in}; (a) M_{in}= 6 mg/s and (b) M_{in}= 10 mg/s

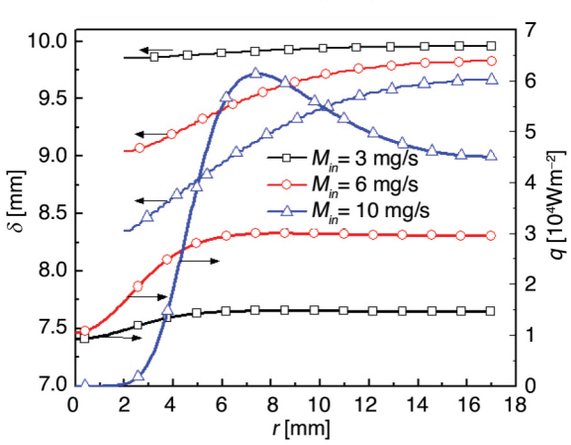

Figure 9. Distribution of δ and q along the radial direction

The contours of phase under different mass flow rate min is shown in fig. 8, where T_{sat} = 650 K, T_w = 646 K, and the distribution of δ along the radial direction is given in fig. 9. It is obvious that the entire vapor-liquid interface moves into the porous wick as the M_{in} increases, meanwhile, the moving distance decreases along the radial direction. This suggests that the porous wick condenser can meet the requirement of steady condition by adjusting the position and shape of the interface. In this way, the heat transfer area is increased, and the decreasing thickness

of liquid sodium can also reduce the heat transfer resistance, thus the condensation process is enhanced. However, this self-adaptive ability is limited. The simulation results indicate that once the mass- flow rate increases to M_{in} = 15 mg/s, the interface front extends to the outlet, suggesting that some uncondensed sodium vapor flow into the liquid-return artery, and the condenser reaches its working limitation. Additionally, distributions of q show similar tendency under different M_{in}, *i.e.*, q increases initially and then decreases along the radial direction as shown in fig. 9. However, the decreasing δ increases the inhomogeneity of the cold end heat flux q. When M_{in} = 10 mg/s, the q at a small r is close to 0, and changes more sharply along the radial direction.

The effect of cold wall temperature

Under an ideal working situation, the vapor-liquid in-terface is expected to stay steady on the surface of the porous wick condenser. This interface reduces radiative heat losses to the condenser because of its high reflectivity. The cold wall temperature, T_w, is a key parameter to determine the amount of condensation and the shape of the interface directly.

Figure 10 illustrates the distribution of liquid sodium thickness film along the radial direction under different T_w, when M_{in} = 10 mg/s. It can be found that the interface front goes deep into the porous wick when T_w = 646 K, the thickness of liquid sodium film δ increases along the decreasing temperature and the lower T_w causes a smaller growth rate of δ. When T_w = 639 K, the interface is close to an ideal state, the film thickness varies slightly along the radial direction, which is similar to the distribution in fig. 6(a) (M_{in} = 3 mg/s, T_w = 646 K). It means that there is a corresponding T_w for a certain M_{in} to ensure the stable vapor-liquid interface inside the porous wick condenser. Besides, the greater the mass-flow rate becomes, the smaller this corresponding T_w is. It should be noted that, if the T_w continue to decrease after reaching optimal value, the sodium vapor will condensate before getting to the porous wick, thus make the pressure in the low pressure cavity fluctuate strongly. This is not allowed in the actual operation. In addition, fig. 10 shows the distribution of q along the radial direction, the lower T_w causes a smaller peak value and a more uniform distribution of q.

The effect of distance between artery and cold end

All the previous results are obtained under the condition that the distance between artery and cell wall L_{cd} is 5 mm. This section will study the effect of L_{cd} on the performance of the condenser under the operation condition that T_{sat} = 650 K, T_w = 646 K, M_{in} = 3 mg/s, and the L_{cd} is taken to be 3 mm, 2 mm respectively.

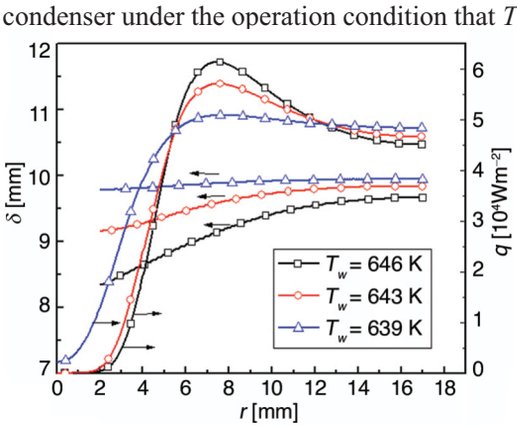

Figure 10. Distribution of δ and q along the radial direction (M_{in} = 10 mg/s)

Figure 11 shows the contours of temperature under different L_{cd}, it can be seen that changing the distance between artery and cell wall has little effect on the temperature field in the porous wick, but it has a significant influence on the temperature distribution at the outlet compared with the fig. 6(b). As shown in fig. 12, the outlet temperature increases gradually along the radial direction, and the smaller the L_{cd}, the lower the T_{out}. Actually, the T_{out} is always expected to be lower. It is due to that heat input of the hot end will heat liquid sodium in the artery, and the capillary evapora-

tor may become dry if this heat input is too large. The lower temperature of liquid sodium can reduce the dry-out risk of evaporator. It is also shown that changing the distance has little impact on the distribution of δ as is shown in fig.13. Hence the performance of AMTEC is enhanced by a smaller L_{cd}.Besides, the distance L_{cd} also influences the distribution of cold end heat flux q as swown in fig. 13. Althout the general distibutions od q under different L_{cd} are similar, the peak value of q increases with the decreasing L_{cd}, and radial location where the maximum q appears moves to the centre as the L_{cd} reduces.

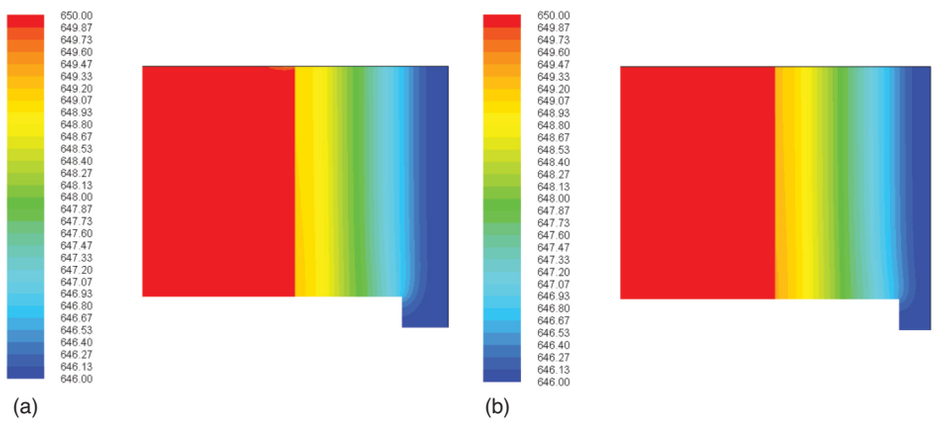

Figure 11. Contours of temperature under different L_{cd} ; (a) L_{cd} = 3 mm and (b) L_{cd} = 2 mm

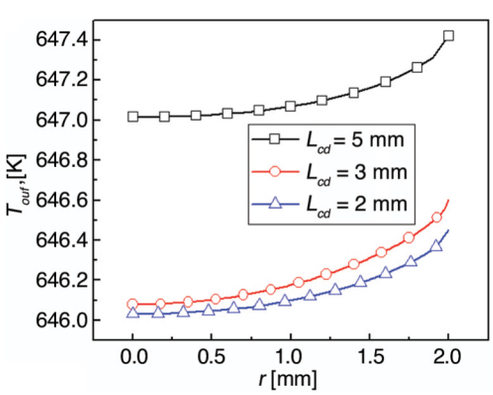

Figure 12. Temperature distribution at the outlet T_{out} under different L_{cd}

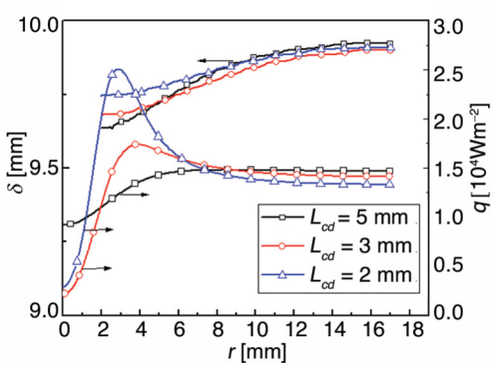

Figure 13. Distribution of δ and q along the radial direction

Conclusions

The porous wick condenser is an important component which controls the circulation, heat and mass transfer of AMTEC. In this paper, a physical and mathematical model for the sodium vapor condensation heat transfer of the AMTEC porous wick condenser was established. Through numerical simulation, the steady-state distributions of physical fields were obtained and the influences of the relevant parameters on the condensation heat transfer characteristics were discussed.

The results reveal that, for an ideal working situation, the thickness of liquid sodium film, δ, increases gradually along the radial direction, the temperature distribution in liquid phase is approximately linear, while the temperature in vapor is constant. Moreover, the condensation

rate of sodium vapor on the phase-change interface decreases along the radial direction, and the cold end heat flux increases initially and then decreases along the radial direction. The porous wick condenser has very limited self-adaptive ability once the mass- flow rate, M_{in}, increased. In addition, there is a corresponding T_w for a certain M_{in} to ensure the stable phase-change interface in the porous wick condenser. The greater the mass-flow rate becomes, the smaller the corresponding T_w is. Finally, changing the distance between artery and cell wall has significant influences on the outlet temperature and the cold end heat flux. The performance of AMTEC can be enhanced by a smaller L_{cd}.

Acknowledgement

This work is supported by National Natural Science Foundation of China (Project No.51306215).

Nomenclature

c – heat capacity [Jkg^{-1}K^{-1}]
D – variable differentiating the low pressure cavity and the porous wick
h_{fg} – latent heat [Jkg^{-1}]
K – permeability [m^2]
$\dot{m}$ – mass production rate of condensation [kgm^{-3}s^{-1}]
M_{in} – mass-flow at inlet [kgs^{-1}]
L_{cd} – distance between artery and cold end [mm]
P – pressure [Pa]
P_{out} – pressure at outlet [Pa]
Q – heat transfer rate [W]
Q' – calculated total heat transfer rate [W]
r – radial co-ordinate [mm]
r_p – effective aperture [m]
S_h – energy source term [Jm^{-3}s^{-1}]
T – temperature [K]
T_{sat} – saturation temperature [K]
t – time [s]
V – superficial velocity [ms^{-1}]
z – axial co-ordinate [mm]

Greek symbols
α – volume fraction
δ – thickness of liquid film [mm]
β – mass transfer intensity factor
ε – porosity
λ – thermal conductivity [Wm^{-1}K^{-1}]
λ_{eff} – effective thermal conductivity [Wm^{-1}K^{-1}]
μ – viscosity [kgm^{-1}s^{-1}]
ρ – density [kgm^{-1}]

Subscript
f – working fluid
in – inlet
l – lliquid phase
out – outlet
s – solid phase
sat – saturation state
v – vapor phase
w – wall

References

[1] Lodhi, M. A. K., *et al*., An Overview of Advanced Space/Terrestrial Power Generation Device: AMTEC, *Journal of Power Sources*, *103* (2001), 1, pp. 25-33
[2] Wu, S. Y., *et al*., A Review on Advances in Alkali Metal Thermal to Electric Converters (AMTECs), *International Journal of Energy Research*, *33* (2009), 10, pp. 868-892
[3] Svedberg, R. C., *et al*., Heat Shields for Alkali Metal Thermal to Electric Conversion (AMTEC) Cells, United State Patent, 1999
[4] Tournier, J., El-Genk, M. S., Performance Analysis of Pluto/Express, Multitube AMTEC Cells, *Energy Conversion & Management*, *40* (1999), 2, pp. 139-173
[5] Tournier, J. M., *et al*., AMTEC Performance and Evaluation Analysis Model (APEAM): Comparison with Test Results of PX-4C, PX-5a, and PX-3a Cells, *AIP Conference Proceedings*, *420* (1998), 1, pp. 1576-1585
[6] El-Genk, M. S., Tournier, J. M. P., Analyses of Static Energy Conversion Systems for Small Nuclear Power Plants, *Progress in Nuclear Energy*, *42* (2003), 3, pp. 283-310
[7] El-Genk, M. S., Tournier, J. M., Performance Comparison of Potassium and Sodium Vapor Anode, Multi Tube Amtec Converters, *Energy Conversion & Management*, *43* (2002), 15, pp. 1931-1951
[8] Lodhi, M. A. K., Daloglu, A., Performance Parameters of Material Studies for AMTEC Cell, *Journal of Power Sources*, *85* (2000), 2, pp. 203-211

[9] Wu, S. Y., *et al*., Influence of Working Fluids and Wick Materials on Performance of Porous Wick Evaporator Based on AMTEC, *Journal of Engineering Thermophysics*, *33* (2012), 12, pp. 2150
[10] Wu, S. Y., *et al*., Parametric Study on Flow and Heat Transfer Characteristics of Porous Wick Evaporator Based on AMTEC, *Journal of Mechanical Science and Technology*, *26* (2012), 3, pp. 973-981
[11] El-Genk, M. S., King, J. C., Performance Analyses of an Nb-1Zr/C-103 Vapor Anode Multi-Tube Alkali-Metal Thermal-to-Electric Conversion Cell, *Energy Conversion & Management*, *42* (2001), 6, pp. 721-739
[12] Mohamed, E. M., Rashed, A., Film Condensation Generated by Free Convection in a Porous Medium, *Thermal Science*, *22* (2018), 6, pp. 2699-2710
[13] Wang, S. C., *et al*., Steady Filmwise Condensation with Suction on a Finite-Size Horizontal Flat Plate Embedded in a Porous Medium Based on Brinkman and Darcy Models, *International Journal of Thermal Sciences*, *45* (2006), 4, pp. 367-377
[14] Chang, T. B., Laminar Filmwise Condensation on Horizontal Disk Embedded in Porous Medium with Suction at Wall, *Journal of Heat Transfer*, *130* (2008), 7, pp. 351-358
[15] Annamalai, A. S., Ramalingam, V., Experimental Investigation and Computational Fliud Dynamics Analysis of an Air Cooled Condenser Heat Pipe, *Thermal Science*, *15* (2011), 3, pp. 759-772
[16] Chang, T. B., Yeh, W. Y., Theoretical Investigation into Condensation Heat Transfer on Horizontal Elliptical Tube in Stationary Saturated Vapor with Wall Suction, *Applied Thermal Engineering*, *31* (2011), 5, pp. 946-953
[17] Alizadehdakhel, A., *et al*., CFD Modeling of Flow and Heat Transfer in a Thermosyphon, *International Communications in Heat and Mass Transfer*, *37* (2010), 3, pp. 312-318
[18] Zhang, Y., *et al*., Capillary Blocking in Forced Convective Condensation in Horizontal Miniature Channels, *Journal of Heat Transfer*, *123* (2001), 3, pp. 501
[19] Liu, Z., *et al*., VOF Modeling and Analysis of Filmwise Condensation Between Vertical Parallel Plates, *Heat Transfer Research*, *43* (2012), 1, pp. 47-68
[20] Yang, Z., *et al*., Numerical and Experimental Investigation of Two Phase Flow During Boiling in a Coiled Tube, *International Journal of Heat & Mass Transfer*, *51* (2008), 5, pp. 1003-1016
[21] Riva, E. D., Col, D. D., Effect of Gravity During Condensation of R134a in a Circular Minichannel *Microgravity Science and Technology*, *23* (2011), 1, pp. 87-97
[22] Zang, H., *et al*., *Heat Pipe Energy-saving Technology* (in Chinese), Chemical Industry Press, Beijing, China, 2009
[23] Liu, Z. C., *et al*., Numerical Simulation of Two Phase Flow and Heat Transfer in CPL Condenser with Porous Element, *Journal of Engineering Thermophysics*, *28* (2007), 2, pp. 81-84
[24] Qu, Y., , *Flow and Heat Transfer Characteristics in the Porous Wick Condenser of CPL* (in Chinese), Beijing: Tsinghua university, China, 2000
[25] Shi, M.H., *et al*., *Boiling and Condensation* (in Chinese), Higher Education Press, Beijing, China, 1995

Paper submitted: July 27, 2017
Paper revised: February 04, 2018
Paper accepted: February 11, 2018